THE JOURNAL OF BIOLOGICAL CHEMISTRY VOL. 283, NO. 5, pp. 2709–2715, February 1, 2008

Four-turn α-Helical Segment Prevents Surface Expression of the Auxiliary hβ2 Subunit of BK-type Channel*

Received for publication, May 30, 2007, and in revised form, October 19, 2007 Published, JBC Papers in Press, November 8, 2007, DOI 10.1074/jbc.M704440200

Caixia Lv[‡1], Maorong Chen[‡1], Geliang Gan[‡1], Lifen Wang[‡], Tao Xu[‡§2], and Jiuping Ding[‡3]

From the [‡]Key Laboratory of Molecular Biophysics (Huazhong University of Science and Technology), Ministry of Education, Wuhan, Hubei 430074, China and the [§]National Laboratory of Biomacromolecules, Institute of Biophysics, Chinese Academy of Science, Beijing 100101, China

Large conductance, voltage- and Ca^{2+}-activated K^+ (BK) channels encoded by the mslo α and β2 subunits exist abundantly in rat chromaffin cells, pancreatic β cells, and DRG neurons. The extracellular loop of hβ2 acting as the channel regulator influences the rectification and toxin sensitivity of BK channels, and the inactivation domain at its N terminus induces rapid inactivation. However, the regulatory mechanism, especially the trafficking mechanism of hβ2, is still unknown. With the help of immunofluorescence and patch clamp techniques, we determine that the hβ2 subunit alone resides in the endoplasmic reticulum, suggesting that trafficking mechanism of hβ2 differs from that of hβ1 opposite to what we predicted previously. We further demonstrate that a four-turn α helical segment at the N terminus of hβ2 prevents the surface expression of hβ2, that is, the helical segment itself is a retention signal. Using the c-Myc epitope-tagged extracellular loop of hβ2, we reveal that the most accessible site by antibody is located at the middle of the extracellular loop, which might provide clues to understand how the auxiliary β subunits regulates the toxin sensitivity and the rectification of BK-type channels.

Large conductance voltage- and Ca^{2+}-activated K^+ (BK)[4] channels associated with its auxiliary β subunits show functional varieties in many native cells (1–13). The auxiliary β1–β4 subunits of BK channels are composed of two transmembrane segments and a large extracellular segment (5, 14–16). For hβ2 subunits, three hydrophobic residues FIW at its N terminus produces a rapid inactivation of BK channels (15), whereas it does not follow a typical N-type inactivation mechanism (17). The NMR experiment reveals a four-turn helix structure located at the middle of its N terminus (24). Recently, Zhang *et al.* (18) reported that trypsin can easily target the Arg^8 and Arg^9 of nine basic residues before the helix. In addition, its extracellular loop prevents the scorpion toxin charybdotoxin from approaching the channel pore (9) and induces the rectification of BK channels (19). It has been reported that the β1 and β2 subunits contain endocytic sorting signals at their C termini, which can down-regulate the association MaxiK channel surface expression levels (14, 20). The β1 subunit can reach the cell membrane alone, whereas the β2 subunit only appears underneath the plasma membrane (14, 20, 21). Obviously, the trafficking mechanism of hβ2 subunits is still unknown so far.

There are many mechanisms for governing the surface expression of ion channels and thus the electrical activity of a cell. A channel protein in a misfolded or unfolded state can be trapped in the ER as demonstrated by measurements of the surface labeling, luminomitry. Some retrieval/retention and anterograde signals determine the ER exit of proteins (22). The retention sequence RKR appearing in potassium inward rectifying channel (Kir) and its auxiliary SUR1 subunit is due to improperly folded or assembled channels (22, 23). Both the Kir and SUR1 subunits have the cytosolic RKR sequences, which must be masked by the assembly of octamer before channels can be transported to the cell surface (23). Zarei *et al.* (24) also report that a nonbasic hydrophobic retention/retrieval motif CVLF prevents the surface expression of mslo α and β1-subunits.

With the help of immunofluorescence and patch clamp techniques, we find that the auxiliary hβ2 subunit cannot traffic to the cell surface without associating with the mslo α subunit. Fortunately, the hβ2 subunit can solely traffic to the cell surface only after demolishing or destroying a four-turn α helical segment of its N terminus (25), which may implicate a novel trafficking mechanism. We also find that the most accessible region by antibody is located at the middle position of the hβ2 outer loop near the channel filter, suggesting that it may be the important site in regulating the toxin sensitivity and rectification of inactivating BK currents.

MATERIALS AND METHODS

Constructions and Mutagenesis—The full-length cDNA for each of the mslo α or hβ2 were subcloned into pcDNA3.1/Zeo(+) (Invitrogen). For the construct hβ2-Tdimer2, hβ2 cDNA, and Tdimer2 cDNA were subcloned into pcDNA3.1/Zeo(+). The BK pore-forming α subunit (mslo) was tagged with the c-Myc epitope (EQKLISEEDL) at the N terminus. To get a green fluorescence protein targeted ER, pEGFP-ER, the enhanced green fluorescence protein (EGFP) was used to substitute the DsRed2 in pDsRed2-ER (Clontech). The human β subunits (hβ1/hβ2) were tagged with epitope (c-Myc,

* This work was supported by National Science Foundation of China Grants 30470449, 30470646, 30630020, and 30670502. The costs of publication of this article were defrayed in part by the payment of page charges. This article must therefore be hereby marked "*advertisement*" in accordance with 18 U.S.C. Section 1734 solely to indicate this fact.

[1] These authors contributed equally to this work.

[2] To whom correspondence may be addressed. Tel.: 86-10-648-884-69; Fax: 86-10-648-675-66; E-mail: xutao@ibp.ac.cn.

[3] To whom correspondence may be addressed. Tel.: 86-27-877-921-53; Fax: 86-27-877-920-24; E-mail: jpding@mail.hust.edu.cn.

[4] The abbreviations used are: BK, large conductance voltage- and Ca^{2+}-activated K^+; ER, endoplasmic reticulum; EGFP, enhanced green fluorescence protein.

EQKLISEEDL; hemagglutinin, YPYDVPDYA) at different positions of the putative extracellular loop by sequential overlap extension PCR. Series of constructs for deletions of the hβ2–137myc N terminus were made by deleting appropriate amino acids from hβ2–137myc and introducing a new start codon with PCR primers. The mutations on hβ2–137myc were created with the QuikChange site-directed mutagenesis kit (Stratagene). All of the constructs and mutations were verified by direct DNA sequence analysis.

Immunofluorescence Imaging in HEK293 Cells—HEK293 cells were cultured in Dulbecco's modified Eagle's medium supplemented with 10% fetal bovine serum, 100 IU/ml penicillin, and 100 IU/ml streptomycin. The cells were transiently transfected using Lipofectamine 2000 (Invitrogen). After transfection, the live cells were transferred to a poly-D-lysine-coated chamber. The next day, the cells were fixed with 2% paraformaldehyde in phosphate-buffered saline for 5 min. For cell permeabilization, 0.2% Triton X-100 was added for 5 min. After blocked with 5% goat serum for 1 h, the cells were incubated with a monoclonal anti-human c-Myc antibody (1:200) for 3 h, washed, and incubated with fluorescein isothiocyanate-conjugated anti-mouse IgG (H+L) (1:150) for 1 h. All of the experiments were performed at room temperature (22–25 °C). Mouse anti-human c-Myc and fluorescein isothiocyanate rabbit anti-mouse IgG (H+L) conjugate were purchased from Zymed Laboratories Inc.

We took advantage of the high numeric aperture objective (APO ×100 OHR, NA = 1.65, Olympus) to take high resolution fluorescence images of transfected cells. Excitation light from a fiber optical coupled monochromator (Polychrome IV; TILL Photonics GmbH, Germany) was passed through a shutter that opened only during camera exposure. The wavelength selection and switch were controlled by the image acquiring software (TILL vision 4.0; Till Photonics GmbH). The images were acquired with a cooled CCD (PCO SensiCam; Germany) with pixel size of 0.067 μm at the specimen plane.

Image Analysis and Statistics—Images were viewed, processed, and analyzed in TILL Vision (TILL.Photonics, Germany) and Adobe Photoshop (Adobe Systems) and IMAGE J (National Institutes of Health, Public Domain). The exposure time was 2000 ms. Control experiments were executed for each batch of experiments. All of the experiments were performed at there different batches. At each batch, every chamber is normalized to the control.

Solutions—HEK293 cells were bathed in ND-96 solution (pH 7.5) containing the following: 96 mM NaCl, 2 mM KCl, 1.8 mM $CaCl_2$, 1 mM $MgCl_2$, 2.5 mM $C_3H_3O_3Na$ (sodium pyruvate), and 10 mM HEPES. For current recording of BK channels, extracellular solution contained the following: 160 mM $MeSO_3K$, 2 mM $MgCl_2$, 10 mM HEPES, pH 7.0, titrated with $MeSO_3H$; intracellular solution contained the following: 160 mM $MeSO_3K$, 10 mM HEPES, 5 mM *N*-hydroxyethylenediaminetriacetic acid with added Ca^{2+} for 10 μM free Ca^{2+} and 5 mM EGTA with no added Ca^{2+} for 0 μM Ca^{2+} solution, as defined by the EGTAETC program (McCleskey, Vollum Institute, Portland, OR), with the pH adjusted to 7.0, titrated by $MeSO_3H$. All of the chemicals were attained from Sigma.

Electrophysiology—Patch pipettes were pulled from borosilicate glass capillaries with a resistance of 2–4 megohms when filled with pipette solution. Inside-out patches were used in experiments. During recordings, 0 and 10 μM Ca^{2+} solutions were applied onto the cell via a perfusion pipette containing seven solution channels. All of these experiments were performed at room temperature (22–25 °C). The experiments were performed using a PC2C patch clamp amplifier with its software (InBio). The currents were typically digitized at 100 kHz. Macroscopic records were filtered at 5 kHz. Patch clamp recording data were analyzed with IGOR (Wavemetrics, Lake Oswego, OR), Clampfit (Axon Instruments, Inc.), and Sigmaplot (SPSS, Inc.) software.

RESULTS

Auxiliary hβ2 Subunits Alone Reside in the ER—The hβ subunits of a four-member β family (hβ1–hβ4) have the similar structure, *i.e.* with two transmembrane segments, an extra large loop, and a few consensus glycosylation sites (26) (Fig. 1*A*). The hβ2 subunits like other β subunits have many ways to regulate the mslo BK channels. For example, its extracellular loop alters the conductance and toxin sensitivity of BK channels, but its N terminus introduces a rapid inactivation of BK channels (9, 17, 19). The hβ1 subunits have been reported and can traffic to the cell surface alone (14). However, it is unclear whether the auxiliary hβ2 subunits also traffic to the plasma membrane as hβ1 subunits do. To investigate the trafficking mechanism of auxiliary hβ2 subunits, a c-Myc epitope was tagged to the center of the loop for measuring the surface expression of hβ2 subunits (Fig. 1*A*). Considering that recognition signals (export and retention/retrieval) of proteins in the ER are mostly found at the N or C termini, we constructed a series of mutations at the N terminus to investigate the trafficking mechanism of the hβ2 subunits (Fig. 1*B*). A three-dimensional structure of the N-terminal helix from 18 to 31 is plotted in the Fig. 1*C* (25).

Because coexpression of mslo α and hβ2 subunits can make the inactivating functional BK channels, we expected that images for coexpression of Myc-mslo (*green*) and hβ2-Tdimer2 (*red*) should show their coexistence in HEK293 cells. In fact, images for Myc-mslo, hβ2-Tdimer2, and Myc-mslo+hβ2-Tdimer2 show green (*left*), red (*middle*), and yellow (*right*) brims, respectively, which indicates coexistence of two proteins on the cell surface (Fig. 2*A*). In contrast, there was no red contour distinctly appearing on the cell brim, whereas the hβ2-Tdimer2 was transfected alone in HEK293 cells. The image of coexpression of pEGFP-ER with hβ2-Tdimer2 demonstrates that two proteins coexist in the ER (Fig. 2*B*). Furthermore, there was no detectable colocalization with coexpression of the hβ2-Tdimer2 with an EGFP-tagged Golgi marker (data not shown) that meant the hβ2 subunit should be retained in ER. Because the Tdimer2 is a protein with more than 450 amino acids, it may influence the traffic of hβ2. To precisely recognize and quantify surface expression of hβ2 subunits, a c-Myc epitope was tagged at the loop. Similarly, the image for coexpression of mslo with hβ2–137myc revealed that the hβ2–137myc subunits were transported to the membrane surface (Fig. 2*C*, *right panel*). It is interesting that the surface signals (*green*) of the hβ2–137myc subunits alone could be detected only under permeabilized

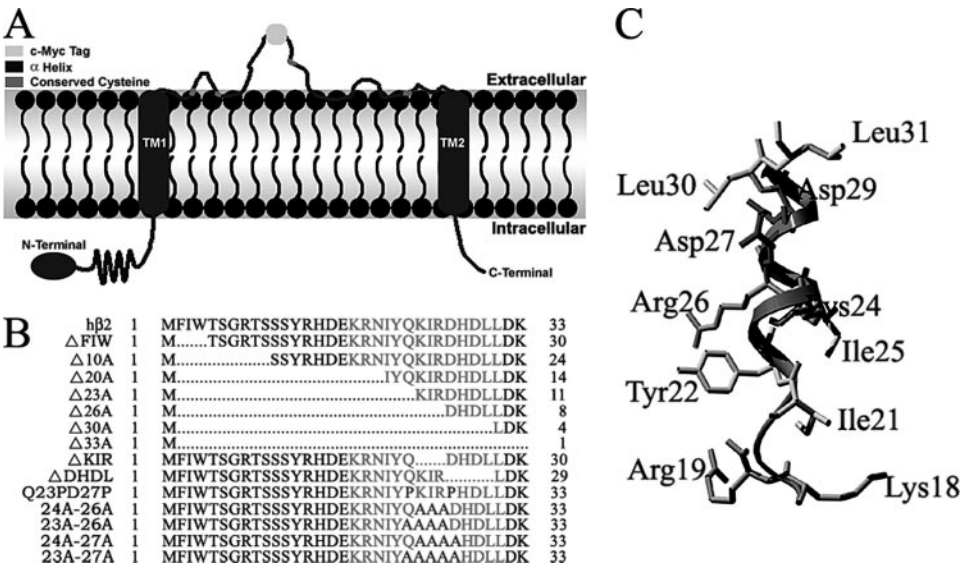

FIGURE 1. **Mutagenesis at the N terminus and extracellular loop of the auxiliary hβ2 subunits of BK channels.** *A*, topology of hβ2 subunits exhibits a putative structure, which consists of a N terminus, two transmembrane domains (*TM1* and *TM2*), a long extracellular loop, and a short C terminus. The N terminus contains three components: an inactivation "ball" domain, am α-helical segment (*dark gray*), and two flexible linkers. Four conserved cysteines (*medium-dark gray*) in the extracellular loop are located to positions 84, 113, 142, and 174, respectively. In most experiments, a c-Myc epitope (*light gray*) was inserted at position 137 of the extracellular loop. *B*, a series of N-terminal mutations and constructs of hβ2 subunits is shown in the list. The residues 18–31 of the α helical segment are labeled in *light gray*, and the substituting residues are in *dark gray*. *C*, a three-dimensional structure of the four-turn helix from 18 to 31 of hβ2 subunits gives more detailed orientation of residues. The hydrophobic residue is labeled in *light gray*, the negatively charged one is in *dark gray*, and the positively charged one is in *medium-dark gray*.

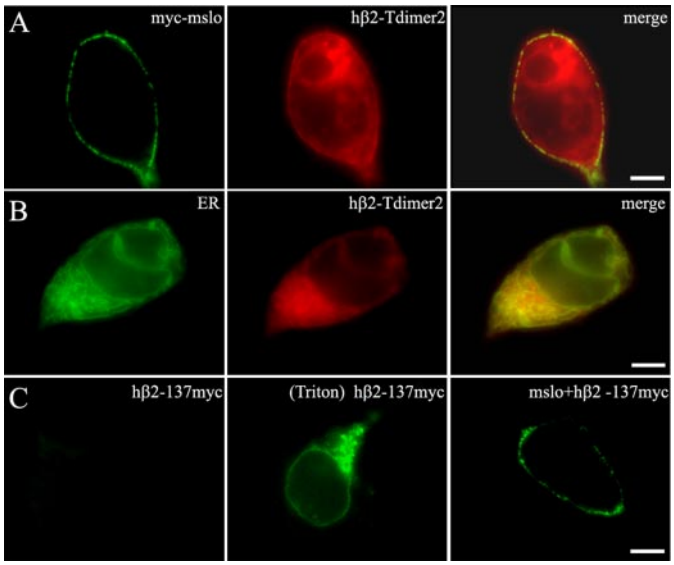

FIGURE 2. **The hβ2 subunits are restricted to the ER.** *A*, HEK293 cells were co-transfected with Myc-mslo (*green*) and hβ2-Tdimer2 (*red*) subunits. Images for Myc-mslo (*left panel*) and hβ2-Tdimer2 (*middle panel*) have clearly *green* and *red brims*, respectively, and the merged image (*right panel*) has a *yellow brim*, which demonstrated a colocalization of two proteins. The *scale bar* indicates 5 μm. *B*, HEK293 cells were co-transfected with pEGFP-ER (*green*) and hβ2-Tdimer2 subunits (*red*). The images for coexpression of pEGFP-ER and hβ2-Tdimer2 subunits demonstrated coexistence of two proteins in ER. The images are representative of 96 (*top panels*); 16, 54, and 53 (*middle panels*); and 81 (*bottom panel*) cells, respectively. The *scale bar* indicates 5 μm. *C*, HEK293 cells were transfected with hβ2–137myc (*green*) subunits under nonpermeabilized conditions, hβ2–137myc subunits with adding Triton under permeabilized conditions, and the mslo+hβ2–137myc subunits, which are shown in the *left*, *middle*, and *right panels*, respectively (see "Experimental Procedures"). The hβ2–137myc subunits alone do not appear at the cell surface under nonpermeabilized conditions (*left panel*) but clusters in ER under permeabilized conditions (*middle panel*). Coexpression of mslo+hβ2-myc137 subunits shows a hβ2 at the cell surface (*right panel*). The *scale bar* indicates 5 μm.

conditions (Fig. 2*C*, *left* and *middle panels*). In other words, the green signals were undetectable under non-permeabilized conditions, whereas the hβ2–137myc subunits were transfected alone in HEK293 cells (Fig. 2*C*, *left panel*). In conclusion, a surprising finding is that the hβ2 subunit cannot traffic to the plasma membrane alone except that it expresses with the mslo α subunits together.

The hβ2 Subunit Is Restricted in the ER by Four-turn α-Helical Segment—To look for the retention signals of hβ2 subunits, we deleted the C terminus (ΔC) first and then the initial three hydrophobic residues FIW (ΔFIW). In Fig. 3*A*, mutations ΔC and ΔFIW failed to relieve hβ2 from being retained in ER, but they did traffic to the cell surface after coexpressing with the mslo subunits (data not shown). After deleting the first 10, 20, and 30 amino acids of N terminus, we found that the construct Δ30A was the only one appearing on the cell surface, which illuminates that the retention signals of the hβ2 subunits must be concealed among the residues ranging from 20 to 29. Examining their fractional intensities plotted in Fig. 3*D*, we further confirmed that only Δ30A could traffic to the cell surface.

The constructs Δ23A, Δ26A, and Δ30A were designed to precisely determine the retrieval signal or domain. After gradually decreasing the intensity of retention signals, we determined that the retrieval signal is a motif of 23–29 amino acids (Fig. 3*B*). To further determine the exact sequence of retention signals, the mutations ΔKIR and ΔDHDL were designed to relieve the retention signal of ER. In Fig. 3*B*, the construct ΔKIR is clearly a better mutation than the construct ΔDHDL for that purpose. It indicated that the motif KIR played a major role in trapping hβ2 in the ER, which is also consistent with the statistical data of the fractional intensities shown in Fig. 3*E*.

Because alanine-scanning mutations from Q23A to L30A did not show any remarkable surface expression (data not shown), we thus inferred that the motif KIR might be only a core of an expanded sequence. Considering that the motif KIR is located within a four-turn α helical segment ranging from residues 18 to 31 (25), we tested whether the whole helix served as a retention signal. A series of mutations, *i.e.* 23A–26A, 24A–26A, 24A–27A, and 23A–27A, were made to flatten the helix (Fig. 3*C*). Furthermore, mutant Q23P,D27P was constructed to destroy the helix by two prolines, because proline residue is usually thought to promote distortions of transmembrane helices (27, 28) (Fig. 3*C*). In Fig. 3 (*E* and *F*), the expressions of 23A–27A is about 30% more than that of 24A–26A or ΔKIR, which indicates that the motif KIR plays a role in trafficking through its secondary structure.

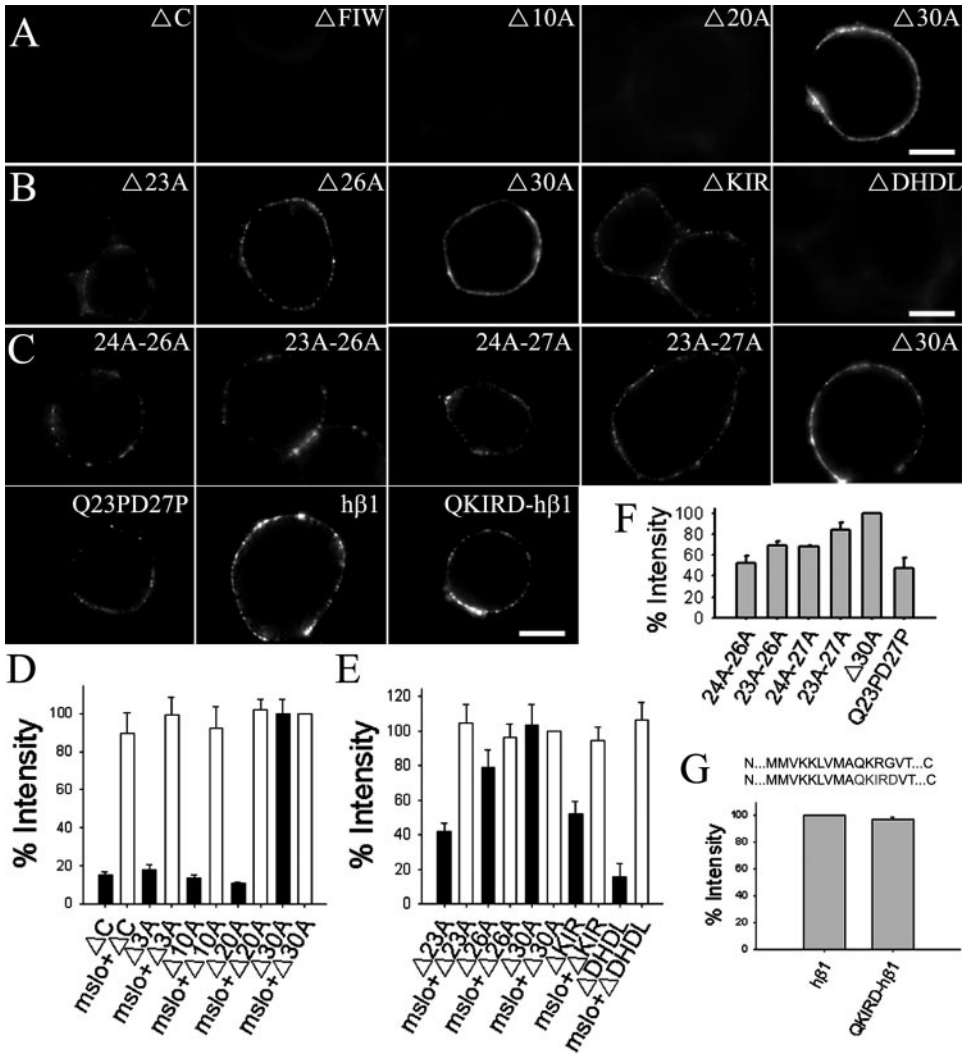

FIGURE 3. **Determination of detention motif of hβ2 at both the N and C termini by site-directed mutagenesis.** *A*, images for HEK293 cells transfected with the constructs ΔC (a C-terminal deletion from Tyr^{221} to Arg^{235}), ΔFIW, Δ10A, Δ20A, and Δ30A tagged with a c-Myc epitope at position 137 are shown. The *scale bar* indicates 5 μm. *B*, images for HEK293 cells transfected with the constructs and mutations Δ23A, Δ26A, Δ30A, ΔKIR, and ΔDHDL tagged with c-Myc epitope at position 137 are shown. The *scale bar* indicates 5 μm. *C*, images for HEK293 cells transfected with the mutations 24A–26A, 23A–26A, 24A–27A, 23A–27A, and Δ30A tagged with c-Myc epitope at position 137 are shown in the *upper panels*. The images for HEK293 cells co-transfected with Q23PD27P, hβ1. and QKIRD-hβ1 (a N-terminal mutation of hβ1) tagged a hemagglutinin epitope at position 98 are shown in the *lower panels*. The *scale bar* indicates 5 μm. *D–G*, the statistical value of fractional pixel intensity is plotted for each mutation as indicated. The fractional intensity of mutations was normalized to the controls mslo+Δ30A (*D* and *E*), Δ30A (*G*), and hβ1 (3*G*), respectively (see "Experimental Procedures"). The percentage intensities of ΔC, mslo+ΔC, ΔFIW, mslo+ΔFIW, Δ10A, mslo+Δ10A, Δ20A, mslo+Δ20A, Δ30A, and mslo+Δ30A are 15.2 ± 1.8 (n = 21), 89.5 ± 10.9 (n = 36), 17.7 ± 3.0 (n = 16), 99.5 ± 8.8 (n = 58), 13.4 ± 1.9 (n = 14), 92.1 ± 11.4 (n = 43), 10.7 ± 0.5 (n = 20), 101.9 ± 5.5 (n = 74), 100.0 ± 7.2 (n = 75), and 100.0 ± 0.0 (n = 68), respectively (*D*). The percentage intensities of Δ23A, mslo+Δ23A, Δ26A, mslo+Δ26A, Δ30A, mslo+Δ30A, ΔKIR, mslo+ΔKIR, ΔDHDL, and mslo+ΔDHDL are 41.9 ± 4.5 (n = 23), 104.7 ± 10.8 (n = 62), 79.0 ± 10.1 (n = 97), 96.4 ± 7.7 (n = 38), 103.5 ± 11.9 (n = 59), 100.0 ± 0.0 (n = 84), 51.9±7.3 (n = 45), 94.3 ± 8.1 (n = 73), 15.8 ± 7.6 (n = 13), and 106.5 ± 10.0 (n = 41), respectively (*D*). The percentage intensities of 24A–26A, 23A–26A, 24A–27A, 23A–27A, Δ30A, and Q23PD27P are 51.9 ± 7.3 (n = 44), 68.8 ± 4.2 (n = 46), 68.1 ± 1.3 (n = 64), 84.2 ± 6.6 (n = 123), 100.0 ± 0.0 (n = 82), and 47.5 ± 9.2 (n = 46), respectively (*F*). The construct QKIRD-hβ1 is shown at the top inset in *G*. The substituting residues are labeled in *gray*. The percentage intensities of hβ1 and QKIRD-hβ1 are 100.0 ± 0.0 (n = 51) and 96.8 ± 1.6 (n = 44), respectively (*G*).

To further demonstrate whether the retention signal is a fixed sequence or a secondary structure, we inserted the QKIRD sequence into the N terminus of hβ1 subunits *i.e.* QKIRD-hβ1 (Fig. 3, *C* and *G*). The mutant QKIRD-hβ1 of hβ1 did not show any clear impact on the surface expression of hβ1 subunits. Therefore, the retention signal of hβ2 subunits is the four-turn helix itself rather than the primary sequence QKIRD. Furthermore, the motif KIR also appears in the βE of the C terminus of mslo subunits (29), which is obviously not a retention signal of BK channels.

To test whether the retention signal at the N terminus was able to present at other locations of hβ2, we translocated the potential retention signal, *i.e.* the first 33 amino acids of N terminus, to the C terminus of hβ2 after Arg^{235} (C33). The C33 alone shows little expression, whereas the mSlo+C33 only shows a little reduction compared with that of the wild type hβ2 (Fig. 4). It means that the same retention signal presents at the new location. We thus believe that the four-turn helix structure at the N terminus is a retention signal of hβ2.

Accessibility of the Extracellular Segment of hβ2 for Antibody Varies with Loci of c-Myc Epitope—We first define the c-Myc antibody accessibility at different positions in the outer segment/loop of hβ2. The differential fluorescence intensity of c-Myc antibody at positions in the hβ2 outer loop may arise from either the cysteine-rich and highly glycosylated structure of the loop or restrictions on access of the big antibody molecule to small volumes. The stronger fluorescence intensity means the c-Myc antibody molecule is easier to reach and bind with its antigen through a more spacious pathway. We thus examined the position dependence of antibody accessibility by inserting c-Myc antigen at different sites in the loop, which was used to provide the detailed structural conformation of the extracellular segment of hβ2.

In addition to the site Lys^{137} in the loop, c-Myc epitope was also introduced either at the C terminus or at the sites 72, 76, 114, 126, 158, and 185 in the loop. However, Lys^{137} is the only site with the clear c-Myc signals in either hβ2 alone or hβ2 with mslo together (Table 1). It is abnormal that we cannot see the c-Myc signals at positions 76 and 158 with coexpression of mslo with hβ2, in the presence or absence of Triton X-100 (Table 1). This may suggest that the mslo α subunit can affect the c-Myc accessibility of hβ2.

To remove the interference of mslo, the construct Δ33A was selected for this purpose. In this construct, the c-Myc epitope

was introduced at the positions 76, 100, 114, 126, 137, 158, and 185 in the loop, respectively. In this work, we found that the positions 126 and 137 are two easiest sites for access of antibody based on their fluorescence intensities, whereas β2 expressed alone (Fig. 5 and Table 1). It indicates that the fluorescence signal at position 126 disappears in the coexpression case. Thus, the c-Myc signal of the hβ2 loop can be covered by the α subunit, specially, by the P-loop of S5–S6 while coexpressed with α subunits.

Because the higher fractional intensity means the higher accessibility of the loop, the most accessible site was plotted at the highest level of the extracellular loop, the second was plotted at the second highest level, and so on. In this way, the "structural" profile of the extracellualr loop can be depicted in a letter "W," of which the apex was located around the middle of the loop (Fig. 5*C*). On the basis of its hydrophobicity plot (9), the hypothetical topology of hβ2 has two transmembrane domains with a large extracellular loop, of which positions 76 and 185 are just located at the N and C termini of the extracellular loop, respectively. Therefore, they should be the easier sites to be approached by antibody. Moreover, the central part of the loop is usually considered to be difficult to approach because it lays over the channel pore and deep into the cell surface (30, 31). According to the above rule of accessibility, the structural profile of the extracellualr loop can be depicted in a letter "M," of which the valley is around the middle too. To our great surprise,

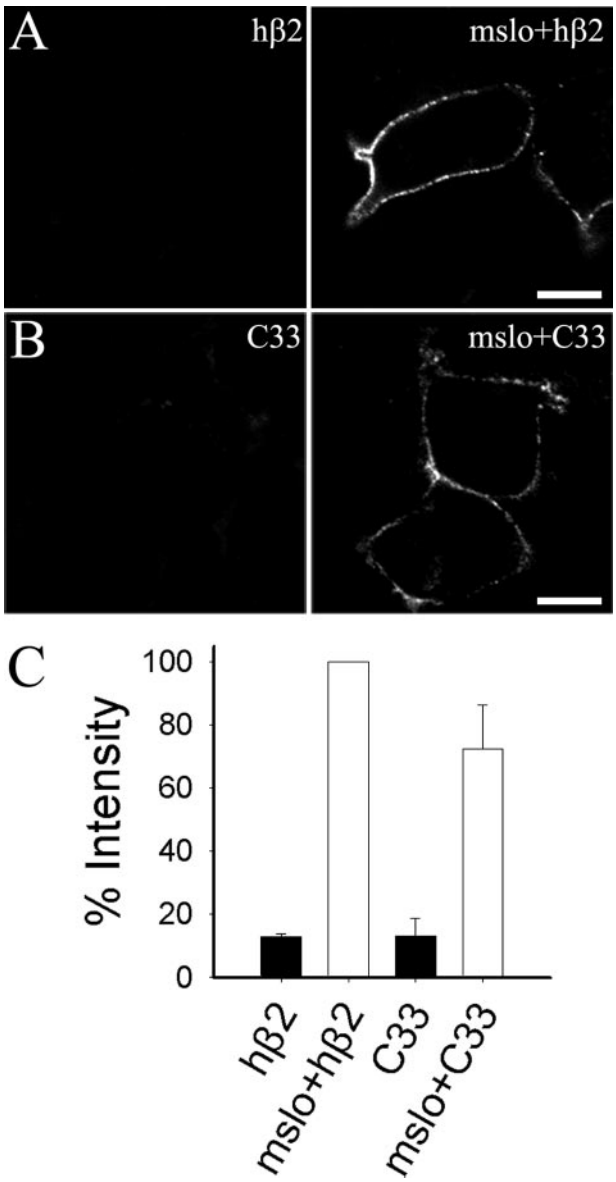

FIGURE 4. **Position dependence of the N-terminal retention signal of hβ2.** *A*, the images for HEK293 cells transfected with hβ2–137myc or mslo+hβ2–137myc. *B*, the images for HEK293 cells expressed with C33 or mslo+C33 (The first 33 amino acids of hβ2 N terminus were translocated to its C terminus after Arg^{235}.) *C*, the percentage intensity of hβ2, mslo+hβ2, C33, and mslo+C33 are 12.8 ± 0.9 (n = 6), 100.0 ± 0.0 (n = 95), 13.0 ± 5.6 (n = 8), and 72.4 ± 13.9 (n = 63), respectively. The *scale bar* indicates 5 μm.

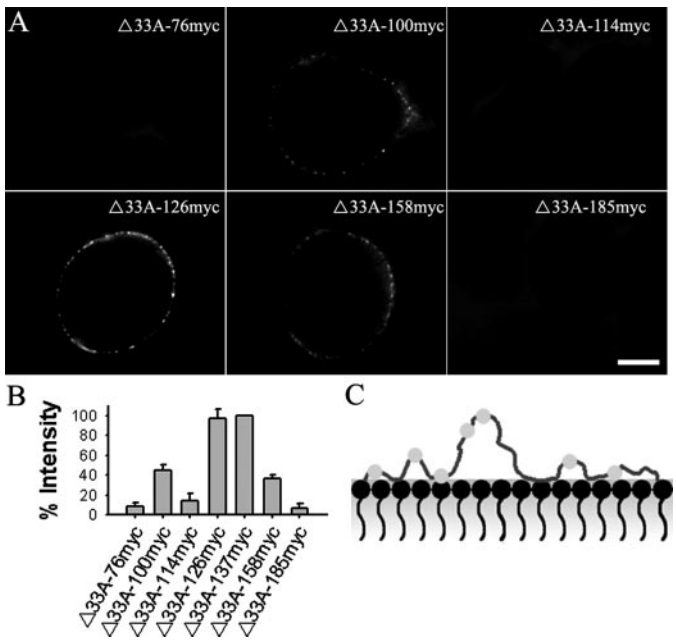

FIGURE 5. **Accessibility of the extracellular loop of hβ2 subunits.** *A*, the images for HEK293 cells transfected with a c-Myc epitope tagged to a construct Δ33A at positions 76, 100, 114, 126, 158, and 185 in the extracellular loop are shown at the *left panel*. The *scale bar* indicates 5 μm. *B*, intensities normalized to that of Δ33A-137myc were plotted for mutations Δ33A with c-Myc epitope tags at different positions 76, 100, 114, 126, 137, 158, and 185 in the loop. The percentage intensities of Δ33A-76myc, Δ33A-100myc, Δ33A-114myc, Δ33A-126myc, Δ33A-137myc, Δ33A-158myc, and Δ33A-185myc are 8.8 ± 4.0 (n = 5), 44.5 ± 6.2 (n = 26), 14.5 ± 7.0 (n = 11), 97.2 ± 9.3 (n = 56), 100.0 ± 0.0 (n = 73), 36.6 ± 3.2 (n = 22), and 6.6 ± 4.8 (n = 7), respectively. *C*, the accessibilities of the extracellular loop by antibodies were plotted based on their fractional intensities indicated in *B*. *Light gray circles* represent the inserted c-Myc epitopes.

TABLE 1
Summary on locations in the P-loop of hβ2 accessible to the c-Myc epitope

Position of c-Myc	72	76	100	114	126	137	158	185	C terminus
hβ2 (no Triton)	No	No	No	No	No	No	No	No	No
hβ2 (Triton)	Yes	Yes	Yes	Yes	Yes	Yes	Yes	Yes	Yes
mslo+hβ2 (no Triton)	No	No	No	No	No	Yes	No	No	No
mslo+hβ2 (Triton)	Yes	No	Yes	Yes	Yes	Yes	No	Yes	Yes

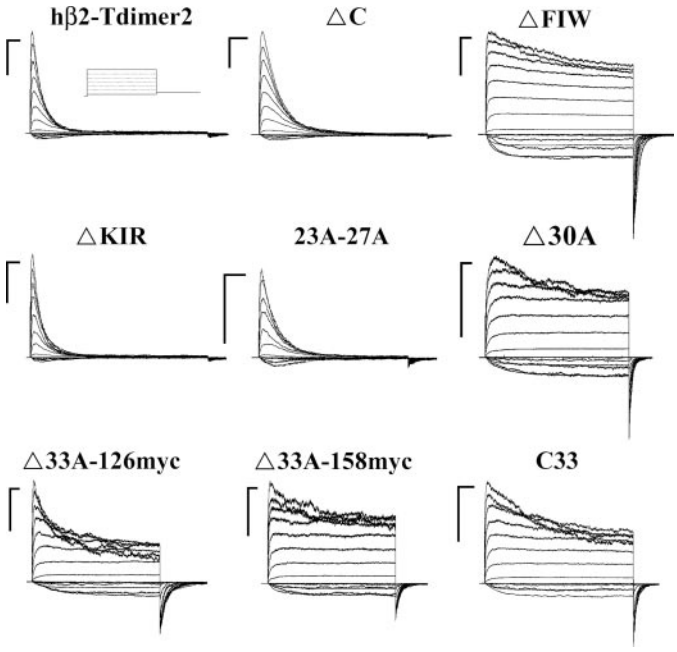

FIGURE 6. **All of the BK channels encoded with mslo and mutations of hβ2 subunits make functional currents.** All of the currents encoded by mslo and hβ2 mutation subunits were recorded in inside-out patches in presence of intracellular 10 μM Ca^{2+}. The traces of mslo+hβ2-mutations were evoked by a voltage step from a holding potential of −180 mV to voltages ranged from −150 to 150 mV in an increment 20 mV. The *scale bars* represent 30 ms (time) and 2 nA (current), respectively. The voltage protocol is plotted on the *upper left*.

the accessibility plotted in Fig. 5*C* completely contradicts our expectation.

All Mutations of hβ2 Maintain Physiological Functions—Another way for validating the surface expression of mutations is to test currents of all the mslo+mutations by voltage clamp experiments. To make it simpler, the representative traces are only coming from some of the mutations (Fig. 6). Typically, mutations with the initial three hydrophobic residues FIW at their N termini always show a rapid inactivation with a time constant of about 25 ms at 100 mV in 10 μM Ca^{2+}. The rest exhibits the larger inward currents at negative voltages, which indicates that there is a huge negative shift (usually more than 50 mV) in conductance-voltage (G-V) curves relative to the G-V curve of mslo α channels. The above results indicate that the hβ2 including its mutations that we constructed in this study can traffic onto the membrane surface of cells after being functionally associated with mslo α subunits.

DISCUSSION

Among β-subunit trafficking, β1 subunit can traffic to the cell surface alone (14, 21), whereas β2 subunit can reach the plasma membrane with the α subunit together. Through the biotinylation experiments, Jin *et al.* (32) reported that the β4 subunit could target to the cell membrane based on the existence of double glycosylation sites in β4 subunits. There is no information about trafficking about β3 subunit so far. Furthermore, Zarei *et al.* (14, 20) observed a putative endocytic signal in the C terminus of the hβ2, which reduced the surface expression of the coexpressed hslo subunits. With polyclonal antibody against β2 subunit using the permeabilized labeling protocol, they found that the hβ2 alone appeared to reach the plasma membrane. We infer that the hβ2 alone stays on the ER membrane just underneath the plasma membrane.

In this study, we were attempting to determine a retention motif in hβ2 like the RXR in potassium inward rectifying channel (Kir) and its auxiliary SUR1 (22, 23) or the CVLF in BK splice variant (24). There are many reasons against KIR being a retention signal. For instance, the surface expression of Δ29A is more than that of Δ26A; QKIRD-hβ1 or Q23PD27P can traffic to membrane surface. Therefore, the second structure of the hβ2 N-terminus is our exclusive choice.

Using NMR spectroscope, Bentrop *et al.* (25) investigated the solution structure of the hβ2 N terminus (amino acids 1–45, BKβ2N). The BKβ2N structure comprises two domains connected by a flexible linker: the ball domain (formed by residues 1–17) and the chain domain (between residues 20–45) linking it to the membrane segment of hβ2. The chain domain consists of a four-turn helix including a 3_{10}-helix (between residues 18–31) with an unfolded linker at its C terminus. The BKβ2N with a four-turn helix is a properly folded peptide as it can functionally inactivate BK channels when applied to the cytoplasmic side (25). Furthermore, our results suggest that the retention signal may be derived from protein-protein or protein-lipid mechanism. Because there is no report about the specific anchoring protein of hβ2, we would rather consider a protein-lipid mechanism. From the three-dimensional structure of the four-turn helix shown in Fig. 1*C* (25), we found that the positively charged residues (Lys^{18}, Arg^{19}, and Arg26) were clustering on one side, and the hydrophobic residues (Ile^{21}/Tyr^{22} and Leu^{30}/Leu^{31}) are lining on each side. Considering that the head group of phospholipid is negatively charged and the tail domain is hydrophobic, we infer that the resultant force coming from electric field and hydrophobic interaction may distort the helix itself to lead the hβ2 subunit coming off the membrane of the ER completely. Furthermore, the positively charged residues Lys and Arg seem to play a crucial role, because the reduction in the number of positively charged residues would somehow weaken the protein-lipid interaction.

It is well known that trypsin can attack and cleave any exposed basic residue in the hβ2 N terminus. Zhang *et al.* (18) reported that the first four basic residues, *i.e.* Arg^{8}, Arg^{14}, Lys^{18}, and Arg^{19}, had the highest trypsin accessibility of basic residue. During hβ2 assembling with mslo in the ER, the C terminus of mslo α subunit may somehow wrap the N-terminal helix of hβ2 to avoid trypsin attack (18). Correspondingly, β subunits reciprocally modulate many properties of BK α channels by the loop-loop interaction of α and β subunits. For instance, the BK α+hβ4 channel is becoming very resistant to CTX or IbTX because of the glycosylation in the loop domain of hβ4 subunits, which prevents the access of toxins to the channel vestibule (32). The outward rectification of BK α+hβ2 channels can be demolished completely by the c-Myc insert hβ2–137myc (data not shown). This study may provide us a new way to understand the interaction of the BK α subunit and β subunit.

The extracellular loop of hβ2 plays an important role in preventing the toxin from approaching the pore of BK channels (9) and producing the rectification of BK channels (19). However, the lack of the structural information about the extracellular

loop prevents us from precisely determining the interacting or binding sites between the loop of hβ2 and the pore of BK channels. Our results reveal that three locations at 137, 100, and 185 represent the peak and valleys of accessibility of the extracellular loop, respectively, which may provide us with important clues to explore the interacting or binding sites in the future. In addition, four conserved cysteines influence the rectifying and pharmacological characteristics of BK channels via forming disulfide bridges to constitute a specific structure in the extracellular loop, that can be disrupted by 20 mM extracellular dithiothreitol (19). Two cysteine mutations (Cys^2 and Cys^3) were constructed for this purpose, whereas we did not find any changes in accessibility. Hopefully, a complete removal of four conserved cysteines may provide more clues for re-evaluating the accessibility of c-Myc antibody to the extracellular loop in the future.

Acknowledgments—We thank Dr. Z. Q. Xu for valuable comments on the manuscript and Dr. C. L. Lingle for kindly providing us with the β1–β4 clones.

REFERENCES

1. Ding, J. P., Li, Z. W., and Lingle, C. J. (1998) *Biophys. J.* **74,** 268–289
2. Brenner, R., Jegla, T. J., Wickenden, A., Liu, Y., and Aldrich, R. W. (2000) *J. Biol. Chem.* **275,** 6453–6461
3. Brenner, R., Perez, G. J., Bonev, A. D., Eckman, D. M., Kosek, J. C., Wiler, S. W., Patterson, A. J., Nelson, M. T., and Aldrich, R. W. (2000) *Nature* **407,** 870–876
4. Dworetzky, S. I., Boissard, C. G., Lum-Ragan, J. T., McKay, M. C., Post-Munson, D. J., Trojnacki, J. T., Chang, C. P., and Gribkoff, V. K. (1996) *J. Neurosci.* **16,** 4543–4550
5. Meera, P., Wallner, M., and Toro, L. (2000) *Proc. Natl. Acad. Sci. U. S. A.* **97,** 5562–5567
6. Nimigean, C. M., and Magleby, K. L. (1999) *J. Gen. Physiol.* **113,** 425–440
7. Tseng-Crank, J., Godinot, N., Johansen, T. E., Ahring, P. K., Strobaek, D., Mertz, R., Foster, C. D., Olesen, S. P., and Reinhart, P. H. (1996) *Proc. Natl. Acad. Sci. U. S. A.* **93,** 9200–9205
8. Wallner, M., Meera, P., and Toro, L. (1999) *Proc. Natl. Acad. Sci. U. S. A.* **96,** 4137–4142
9. Xia, X. M., Ding, J. P., and Lingle, C. J. (1999) *J. Neurosci.* **19,** 5255–5264
10. Wallner, M., Meera, P., and Toro, L. (1996) *Proc. Natl. Acad. Sci. U. S. A.* **93,** 14922–14927
11. Xia, X. M., Ding, J. P., Zeng, X. H., Duan, K. L., and Lingle, C. J. (2000) *J. Neurosci.* **20,** 4890–4903
12. Li, Z. W., Ding, J. P., Kalyanaraman, V., and Lingle, C. J. (1999) *J. Neurophysiol.* **81,** 611–624
13. Li, W., Gao, S. B., Lv, C. X., Wu, Y., Guo, Z. H., Ding, J. P., and Xu, T. (2007) *J. Cell. Physiol.* **212,** 348–357
14. Toro, B., Cox, N., Wilson, R. J., Garrido-Sanabria, E., Stefani, E., Toro, L., and Zarei, M. M. (2006) *Neuroscience* **142,** 661–669
15. Xia, X. M., Ding, J. P., and Lingle, C. J. (2003) *J. Gen. Physiol.* **121,** 125–148
16. Hu, S., Labuda, M. Z., Pandolfo, M., Goss, G. G., McDermid, H. E., and Ali, D. W. (2003) *Physiol. Genomics* **15,** 191–198
17. Savalli, N., Kondratiev, A., de Quintana, S. B., Toro, L., and Olcese, R. (2007) *J. Gen. Physiol.* **130,** 117–131
18. Zhang, Z., Zhou, Y., Ding, J. P., Xia, X. M., and Lingle, C. J. (2006) *J. Neurosci.* **26,** 11833–11843
19. Zeng, X. H., Xia, X. M., and Lingle, C. J. (2003) *Nat. Struct. Biol.* **10,** 448–454
20. Zarei, M. M., Song, M., Wilson, R. J., Cox, N., Colom, L. V., Knaus, H. G., Stefani, E., and Toro, L. (2007) *Neuroscience* **147,** 80–89
21. Zarei, M. M., Eghbali, M., Alioua, A., Song, M., Knaus, H. G., Stefani, E., and Toro, L. (2004) *Proc. Natl. Acad. Sci. U. S. A.* **101,** 10072–10077
22. Deutsch, C. (2003) *Neuron* **40,** 265–276
23. Zerangue, N., Schwappach, B., Jan, Y. N., and Jan, L. Y. (1999) *Neuron* **22,** 537–548
24. Zarei, M. M., Zhu, N., Alioua, A., Eghbali, M., Stefani, E., and Toro, L. (2001) *J. Biol. Chem.* **276,** 16232–16239
25. Bentrop, D., Beyermann, M., Wissmann, R., and Fakler, B. (2001) *J. Biol. Chem.* **276,** 42116–42121
26. Behrens, R., Nolting, A., Reimann, F., Schwarz, M., Waldschutz, R., and Pongs, O. (2000) *FEBS Lett.* **474,** 99–106
27. Bright, J. N., Shrivastava, I. H., Cordes, F. S., and Sansom, M. S. (2002) *Biopolymers* **64,** 303–313
28. Kuo, A., Gulbis, J. M., Antcliff, J. F., Rahman, T., Lowe, E. D., Zimmer, J., Cuthbertson, J., Ashcroft, F. M., Ezaki, T., and Doyle, D. A. (2003) *Science* **300,** 1922–1926
29. Jiang, Y., Lee, A., Chen, J., Cadene, M., Chait, B. T., and MacKinnon, R. (2002) *Nature* **417,** 515–522
30. Hanner, M., Vianna-Jorge, R., Kamassah, A., Schmalhofer, W. A., Knaus, H. G., Kaczorowski, G. J., and Garcia, M. L. (1998) *J. Biol. Chem.* **273,** 16289–16296
31. Qian, X., Nimigean, C. M., Niu, X., Moss, B. L., and Magleby, K. L. (2002) *J. Gen. Physiol.* **120,** 829–843
32. Jin, P., Weiger, T. M., and Levitan, I. B. (2002) *J. Biol. Chem.* **277,** 43724–43729